

1  
2  
3  
4 **Graphite morphologies from the Borrowdale deposit (NW England, UK):**  
5  
6 **Raman and SIMS data**  
7

8  
9 J.F. Barrenechea <sup>(1)</sup>, F.J. Luque <sup>(1,\*)</sup>, D. Millward <sup>(2)</sup>, L. Ortega <sup>(1)</sup>, O. Beyssac <sup>(3)</sup>  
10  
11 and M. Rodas <sup>(1)</sup>  
12

13  
14 <sup>(1)</sup> Dpto. Cristalografía y Mineralogía, Facultad de Geología, Universidad Complutense de  
15 Madrid, 28040 Madrid, Spain.

16  
17 <sup>(2)</sup> British Geological Survey, Murchison House, West Mains Road, Edinburgh EH9 3LA,  
18 UK.

19  
20 <sup>(3)</sup> Laboratoire de Géologie, CNRS, Ecole Normale Supérieure, 24 rue Lhomond, 75005  
21 Paris, France.

22  
23 <sup>(\*)</sup> Corresponding author: [jluque@geo.ucm.es](mailto:jluque@geo.ucm.es)  
24  
25

26  
27 **Abstract**  
28

29  
30  
31 Graphite in the Borrowdale (Cumbria, UK) deposit occurs as large  
32 masses within mineralized pipe-like bodies, in late graphite-chlorite veins, and  
33 disseminated through the volcanic host rocks. This occurrence shows the  
34 greatest variety of crystalline graphite morphologies recognized to date from a  
35 single deposit. These morphologies described herein include flakes,  
36 cryptocrystalline and spherulitic aggregates, and dish-like forms. Colloform  
37 textures, displayed by many of the cryptocrystalline aggregates, are reported  
38 here for the first time from any graphite deposit worldwide. Textural  
39 relationships indicate that spherulitic aggregates and colloform graphite formed  
40 earlier than flaky crystals. This sequence of crystallization is in agreement with  
41 the precipitation of graphite from fluids with progressively decreasing  
42 supersaturation.  
43  
44  
45  
46  
47  
48  
49  
50

51  
52 The structural characterization carried out by means of Raman  
53 spectroscopy shows that, with the exception of colloform graphite around  
54 silicate grains and pyrite within the host rocks, all graphite morphologies display  
55 very high crystallinity. The microscale SIMS study reveals light stable carbon  
56 isotope ratios for graphite ( $\delta^{13}\text{C} = -34.5$  to  $-30.2\text{‰}$ ), which are compatible with  
57 the assimilation of carbon-bearing metapelites in the Borrowdale Volcanic  
58  
59  
60  
61  
62  
63  
64  
65

1  
2  
3  
4 Group magmas. Within the main mineralized breccia pipe-like bodies, the  
5 isotopic signatures (with cryptocrystalline graphite being lighter than flaky  
6 graphite) are consistent with the composition and evolution of the mineralizing  
7 fluids inferred from fluid inclusion data which indicate a progressive loss of CO<sub>2</sub>.  
8  
9 Late graphite-chlorite veins contain isotopically heavier spherulitic graphite than  
10 flaky graphite. This agrees with CH<sub>4</sub>-enriched fluids at this stage of the  
11 mineralizing event, resulting in the successive precipitation of isotopically  
12 heavier graphite morphologies. The isotopic variations of the different graphite  
13 morphologies can be attributed therefore to changes in the speciation of carbon  
14 in the fluids coupled with concomitant changes in the XH<sub>2</sub>O during precipitation  
15 of graphite and associated hydrous minerals (mainly epidote and chlorite).  
16  
17  
18  
19  
20  
21  
22  
23

24 **Key words:** Graphite, morphology, Raman, carbon isotopes, Borrowdale  
25

## 26 Introduction

27

28  
29  
30  
31 The graphite crystal structure consists of a continuous bidimensional  
32 array of six-fold rings of carbon atoms stacked along the c-axis. Thus, as for  
33 most other minerals with layered structures (e.g. phyllosilicates), the  
34 commonest habits of graphite are platy, flaky or scaly crystals (Kwiecinska  
35 1980; Kavanagh and Schlogl 1988; Jaszczak 1995; Luque et al. 1998).  
36 However, in spite of its layered structure several other morphologies have been  
37 reported both in natural occurrences (rocks and meteorites) and in synthetic  
38 compounds (for instance, cast irons). Among these unusual graphite  
39 morphologies, the most common is spherulites which may occur in many rock  
40 types (Gellatly 1966; Rumble et al. 1982; Duke and Rumble 1986; Katz 1987;  
41 Kvasnitsa et al. 1999; Doroshkevich et al. 2007), as a result of precipitation from  
42 fluids or melts. In addition, spherulitic graphite has also been found in some  
43 chondrites (e.g. Mostefaoui et al. 2000, 2005; El Goresy et al. 2005) and it is a  
44 common morphology developed in cast irons (Cooper et al. 2003; Östberg  
45 2006; and references therein).  
46  
47  
48  
49  
50  
51  
52  
53  
54  
55

56 Fibrous (tubular) graphite has been found in artificially produced carbons  
57 (Jaszczak 1995) as well as in some meteorites (Mostefaoui et al. 2005) and  
58 igneous rocks (Jaszczak et al. 2007). Finally, other graphite morphologies  
59  
60  
61  
62  
63  
64  
65

1  
2  
3  
4 including polyhedral (Gogotsi et al. 2000), columnar, pseudodipyramidal,  
5 pseudodipyramidal-prismatic (Kvasnitsa et al. 1999), and cone-shaped  
6 (Jaszczak et al. 2003, 2007) have been described.  
7  
8

9 The goal of the present paper is to describe the unique diversity of  
10 graphite morphologies occurring in a single paragenesis from the renowned  
11 epigenetic graphite deposit at Borrowdale in the English Lake District (Cumbria,  
12 UK; Fig. 1). The geological setting of this graphite deposit is also unusual,  
13 because it is one of only two known examples of graphite mineralization hosted  
14 by volcanic rocks (Barrenechea et al. 1997; Luque et al. 1998). Morphology of  
15 minerals is governed by crystalline structure and the physico-chemical  
16 conditions prevailing during nucleation and growth. Similarly, some geochemical  
17 features are also dependent upon the conditions of crystal growth. Thus,  
18 combining structural and isotopic characterization of the various graphite  
19 morphologies could help unravel the evolution of the mineralizing process in the  
20 particular environment of the volcanic-hosted deposit at Borrowdale, and more  
21 generally provide key information on graphite deposition from fluids.  
22  
23  
24  
25  
26  
27  
28  
29  
30  
31

### 32 33 **Geological setting** 34

35  
36 The Borrowdale graphite deposit consists of mineralized faults hosted by  
37 andesite lavas and sills belonging to the upper Ordovician (Katian) Borrowdale  
38 Volcanic Group, and by a probably contemporaneous hypabyssal dioritic  
39 intrusion (Millward 2004) (Fig. 1). Previous geological studies of the deposit by  
40 Ward (1876) and Strens (1965) stated that narrow veins and stringers filling the  
41 faults comprise massive graphite and chlorite along with quartz. The richest  
42 deposits are developed at the intersections of the faults where there are steeply  
43 inclined pipe-like bodies up to 1 x 3 m in cross-section and from a few metres to  
44 over 100 m in length (Ward 1876). The pipe-like bodies contain nodular masses  
45 and patches of graphite, typically 1-2 cm across, but ranging from a few  
46 millimetres to 1 m or more; the yellow-brown matrix comprises intensely altered  
47 wall-rock and brecciated quartz.  
48  
49  
50  
51  
52  
53  
54  
55  
56

57 The volcanic rocks are underlain by the Skiddaw Group, a succession of  
58 marine turbiditic mudstones and sandstones, possibly late Cambrian to mid  
59 Ordovician in age, and at least 5000 m thick (Cooper et al. 1995, 2004). Several  
60  
61  
62  
63  
64  
65

1  
2  
3  
4 lines of evidence suggest that Skiddaw Group rocks have contributed to the  
5 geochemical development of later aspects of Lake District geology. In particular,  
6 the presence of garnet phenocrysts in peraluminous rocks in the Borrowdale  
7 Volcanic Group and associated intrusions (Fitton 1972) has been attributed to  
8 the assimilation of pelitic material, most likely from the Skiddaw Group  
9 (McConnell et al. 2002). Sulfur isotope data from sulfides within these volcanic  
10 rocks also support this contention (Lowry et al. 1991). Preliminary data on the  
11 bulk carbon isotopic composition of carbonaceous matter disseminated within  
12 the Skiddaw metapelites are close to -28.5 ‰ (Barrenechea et al. 2008).  
13  
14  
15  
16  
17  
18  
19  
20

## 21 **Analytical methods**

### 22 *Petrographic study*

23  
24  
25  
26  
27  
28 Samples from the graphite ore body and its host volcanic rocks were  
29 studied on polished thin sections with a Zeiss Axiophot microscope using both  
30 transmitted and reflected light. The recognition of graphite morphologies was  
31 complemented with the study of selected samples by scanning electron  
32 microscopy (SEM) on gold-coated fragments using a Jeol JSM6400 microscope  
33 operated at 40 kV.  
34  
35  
36  
37  
38  
39

### 40 *Raman spectroscopy*

41  
42  
43 Raman spectra were collected with a Renishaw INVIA spectrometer at  
44 the Ecole Normale Supérieure (Paris, France) on the polished thin sections  
45 used for the petrographic study. This method allows for measurements in situ  
46 and for the preservation of the textural relationships between graphite and the  
47 rest of the minerals in the assemblage. All the measurements were done  
48 focusing the laser beam beneath the surface of transparent minerals (usually  
49 quartz, chlorite, and epidote) associated with graphite to avoid the mechanical  
50 disruption of the graphite structure at the surface of the thin section due to  
51 polishing (Pasteris 1989; Beyssac et al. 2003). The 514.5 nm wavelength of a  
52 20 mW Spectra Physics Argon laser focused through a Leica DMLM  
53 microscope with a 100x objective (N.A.=0.90) was used for the analyses. A  
54  
55  
56  
57  
58  
59  
60  
61  
62  
63  
64  
65

1  
2  
3  
4 1800 gr/mm and a RENCAM CCD detector were used to disperse and analyze  
5 the signal.  
6

7 Under these conditions the spatial resolution is  $\sim 1 \mu\text{m}$  and the spectral  
8 resolution is close to  $1 \text{ cm}^{-1}$ . Laser power on the sample surface was reduced to  
9 2 mW to avoid radiation damage on graphite. Raman analysis of graphite might  
10 also be affected by polarization effects between the incident laser  
11 electromagnetic field and the structure of graphite. This effect might virtually  
12 enhance the defect bands especially for measurement on the graphite edge  
13 planes. These effects are rather weak with a 514.5 nm wavelength (Tan et al.  
14 2004), and to further attenuate them we used a  $\frac{1}{4}$  wavelength plate before the  
15 microscope which yields a circular polarization of the laser.  
16  
17  
18  
19  
20  
21

22 About twenty spectra of each type of graphite morphology were recorded  
23 to gain an insight into the structural heterogeneity within the sample. Acquisition  
24 time was 10 seconds and 5 accumulations ensured a good signal to noise ratio.  
25 No significant changes were observed in the second order Raman region of  
26 graphite, and thus the study focused on the first order Raman spectra (1100 to  
27  $2000 \text{ cm}^{-1}$ ). The Raman parameters (peak position, band area, and band  
28 intensity) were determined with the computer program PeakFit 3.0 using a Voigt  
29 function.  
30  
31  
32  
33  
34  
35  
36  
37

### 38 *Stable carbon isotope analyses*

39  
40

41 Secondary ion mass spectrometry (SIMS) analyses were performed on  
42 the Cameca ims 1270 ion microprobe in the N.E.R.C. Scientific Services'  
43 Edinburgh Ion Microprobe Facility at the University of Edinburgh. Gold-coated  
44 polished thin sections were analyzed using negative secondary ions sputtered  
45 with a positively charged  $\text{Cs}^+$  beam. The spot size was  $20 \mu\text{m}$ . The results were  
46 checked using the graphite standard USGS24 ( $\delta^{13}\text{C} = -16.05 \text{ ‰}$ ; Coplen et al.  
47 2006). Five measurements were made on the standard at the start and end of  
48 each 20 analyses – thus enabling calibration of the sample measurements  
49 against 10 standard measurements. Under these conditions, the precision of  
50 the point analysis is close to  $0.2 \text{ ‰}$ . The  $\delta^{13}\text{C}$  values are referred to the PDB  
51 standard.  
52  
53  
54  
55  
56  
57  
58  
59  
60  
61  
62  
63  
64  
65

## Graphite morphologies

Graphite in the Borrowdale deposit occurs as subspherical to ellipsoidal aggregates (nodules hereafter) and as irregular patches or small veins within altered volcanic rocks of the Borrowdale Volcanic Group and in an associated hypabyssal dioritic intrusion. Nodules and patches may reach up to 10-15 cm in diameter or major length. Their typical size is 1-2 cm, though nodules up to 1 m have been recorded (Ward 1876; Fig. 2a). Graphite also occurs along fault planes in the volcanic rocks, usually associated with chlorite.

Graphite morphologies recognized within the nodules and patches are widely diverse and include both individual forms and aggregates (i.e. groups of individual forms; Table 1). Platy, flaky or scaly graphite crystals (up to 300  $\mu\text{m}$  long and 50  $\mu\text{m}$  wide) are by far the most abundant ( $\approx 90\%$ ), showing no preferred orientation relative to the margins of the nodules. Locally, composite nodules consisting of both flaky and cryptocrystalline graphite have been recognized (Fig. 2b), with flaky graphite usually surrounding cryptocrystalline graphite; the latter may form bands (i.e. colloform textures) around quartz fragments. In some nodules, thin coatings of flaky graphite on quartz fragments (termed hereafter as encapsulated fragments) have been recognized within cryptocrystalline graphite (Fig. 2c). In addition, cryptocrystalline graphite may form rounded patches within flaky graphite (Fig. 2d) and it also occurs with colloform textures, forming bands and globules dispersed within the host rock (Fig. 2e). Colloform graphite in the host rock can be observed around both silicate and pyrite grains (Fig. 2f).

Along with flaky and cryptocrystalline graphite two other morphological types have been recognized: spherulites and ring-like forms. Spherulites consist of radiating arrays of fibrous graphite crystals. In some cases, minute silicate grains can be observed forming the core of the spherulites. In the Borrowdale deposit, spherulites occur in four different settings: 1) as individual forms, 1-5  $\mu\text{m}$  in diameter, or aggregates disseminated within the volcanic rock (Fig. 3a), 2) as individual forms, 5-40  $\mu\text{m}$  in diameter, within flaky graphite (Fig. 3b), 3) as individual forms, 1-3  $\mu\text{m}$  in diameter, enclosed in encapsulated quartz fragments (Fig. 2c), and 4) as aggregates, 5-10  $\mu\text{m}$  in diameter, associated with chlorite along fault zones (Fig. 3c). Ring-like textures are usually hosted by

1  
2  
3  
4 cryptocrystalline graphite (Fig. 2c) or included within encapsulated fragments.  
5 Rings are 1-2  $\mu\text{m}$  wide and consist of tiny graphite crystallites arranged parallel  
6 to both silicate and sulphide (mainly pyrite) cores.  
7

8  
9 Finally, “graphic-like” intergrowth textures, consisting of thin curved and  
10 tapering graphite flakes within chlorite (Fig. 3d), have been observed in samples  
11 from fault zones within the volcanic rock. In places, graphite in graphite-chlorite  
12 intergrowths shows a vermicular (i.e. worm-like) morphology (Fig. 3e).  
13

14  
15 In addition to these morphologies, the SEM study revealed the presence  
16 of concave disks (dish-shaped aggregates) of graphite (up to 40  $\mu\text{m}$  in  
17 diameter) showing rough surfaces (Fig. 3f).  
18  
19  
20

### 21 22 **Raman data**

23  
24  
25  
26 The Raman spectra of graphite are sensitive to the changes in the  
27 degree of crystal perfection (“crystallinity”) along the basal plane of the graphite  
28 structure (Wopenka and Pasteris 1993) that can be correlated to the in-plane  
29 crystallite size ( $L_a$ ). Thus, the first order Raman spectra of highly crystalline  
30 graphite displays a sharp peak at  $\approx 1580\text{ cm}^{-1}$  (ordered or G band). Two  
31 additional bands at  $\approx 1350\text{ cm}^{-1}$  and  $1620\text{ cm}^{-1}$  (D1 and D2 bands) are recorded  
32 in the first order Raman spectra of poorly crystalline graphite, the D2 band  
33 occurring as a shoulder on the G band. The intensity and area ratios for the  
34 disorder to order bands decrease with increasing crystallinity (Wopenka and  
35 Pasteris 1993; Beyssac et al. 2003). The most prominent feature in the second-  
36 order Raman spectra of well ordered graphite is a peak close to  $2700\text{ cm}^{-1}$  (S1  
37 band) which splits into two bands. Recent detailed reviews of the physics behind  
38 the Raman spectrum of graphite are provided by Reich and Thomsen (2004)  
39 and Pimenta et al. (2007).  
40  
41  
42  
43  
44  
45  
46  
47  
48  
49

50 All graphite morphologies from the Borrowdale deposit correspond to  
51 structurally well ordered graphite according to the Raman data. The intensity  
52 and area ratios for the D and G bands in the first-order spectra are consistent  
53 with highly crystalline graphite. In addition, no significant changes were  
54 observed in the second order Raman region, all the spectra showing well-  
55 defined shoulders at  $\approx 2685\text{ cm}^{-1}$  on the S1-peak, which is indicative of the  
56 attainment of tri-periodic order in the structure (Lespade et al. 1982).  
57  
58  
59  
60  
61  
62  
63  
64  
65

1  
2  
3  
4 *Flaky graphite*  
5  
6

7 Raman spectra of flaky graphite from Borrowdale display a sharp G band  
8 and weak or absent D1 and D2 disorder bands (Fig. 4a). The intensity and area  
9 ratios for the disorder to order bands ( $R1 = D1/G$  peak intensity ratio, and  $R2 =$   
10  $D1/(G+D1+D2)$  peak area ratio; Beyssac et al. 2002) average 0.04 for R1, and  
11 0.06 for R2 (Table 2). These features of the Raman spectra indicate a high  
12 degree of crystalline perfection along the basal plane of the graphite structure.  
13 The average crystallite size  $L_a$  is in excess of 2000 Å according to the  
14 estimation of Wopenka and Pasteris (1993) which is based on the area ratio of  
15 the D1 to G bands.  
16  
17  
18  
19  
20  
21  
22  
23

24 *Cryptocrystalline graphite*  
25  
26

27 Significant differences were observed in the first-order Raman spectra of  
28 cryptocrystalline graphite occurring in composite nodules in the pipe-like bodies  
29 compared with that found as colloform bands around silicate or sulphide grains  
30 within the volcanic host rocks (Table 2).  
31  
32

- 33  
34  
35 a) Cryptocrystalline graphite in composite nodules displays the Raman  
36 features of highly ordered graphite, that is, small or absent D1 peak  
37 and sharp G band (Fig. 4b). The average values for R1 and R2 are  
38 0.09 and 0.05, respectively. Such values agree with in-plane  
39 crystallite sizes larger than 2000 Å.  
40  
41  
42 b) Colloform graphite around silicate grains in the volcanic host rock  
43 shows Raman spectra corresponding to graphite of lower crystallinity  
44 (Fig. 4c). In particular, the parameters of the first-order spectra R1  
45 and R2 have higher average values (0.23 and 0.25, respectively) than  
46 those calculated for the other morphologies. Such values agree with  
47  $L_a$  crystallite sizes of 200 to 300 Å.  
48  
49  
50 c) Finally, the Raman spectra of colloform graphite around pyrite grains  
51 in the host rock (Fig. 4d) show the highest R1 and R2 average values  
52 (0.26 and 0.28, respectively) and hence the lowest degree of  
53 crystallinity ( $L_a=150-300$  Å).  
54  
55  
56  
57  
58  
59  
60  
61  
62  
63  
64  
65

### *Spherulitic graphite*

The recorded Raman spectra of spherulitic graphite from the Borrowdale deposit also correspond to highly crystalline graphite (Fig. 4e). No differences have been found for spherulites disseminated in the host rocks or within encapsulated quartz fragments. The parameters of the first-order spectra R1 and R2 have average values of 0.07 and 0.06, respectively. Such values agree with average crystallite sizes larger than 2000 Å. Graphite spherulites within flaky graphite were not analysed because they can only be recognized at the surface of the polished thin sections.

### *Graphite in chlorite*

Graphite (both flaky and vermicular) in “graphic”-like intergrowths and graphite spherulites within chlorite shows Raman spectra corresponding to well-ordered graphite (Fig. 4f). However, R1 and R2 values are slightly higher than those for flaky and cryptocrystalline graphite within the nodules, and also compared to spherulitic graphite disseminated in the host rock or enclosed in encapsulated quartz fragments. The parameters of the first-order spectra R1 and R2 have average values of 0.11 and 0.16, respectively. Such values correspond to  $L_a$  crystallite sizes in the range between 1000 and 1500 Å.

### **Stable carbon isotope data**

The stable carbon isotope ratios for the different morphologies analysed are given in Table 3. No data were obtained for some of the morphologies because they were smaller than the spot size of the ion microprobe. It is worth noting that the analyses of each morphological type fall within very narrow ranges. The most abundant morphology within nodules and disseminations (flakes) has one of the heaviest isotopic signatures (average  $\delta^{13}\text{C}_{\text{PDB}} = -30.26$  ‰) for the graphite in the deposit. Such values are close to those found in graphite spherulites within chlorite (average  $\delta^{13}\text{C}_{\text{PDB}} = -30.15$  ‰). By contrast, cryptocrystalline graphite in composite nodules has significantly lighter isotopic signatures (average  $\delta^{13}\text{C}_{\text{PDB}} = -33.70$  ‰) with no apparent zoning across the

1  
2  
3  
4 banded texture (Fig. 5). The lightest carbon isotope ratios correspond to  
5 vermicular graphite within chlorite (average  $\delta^{13}\text{C}_{\text{PDB}} = -34.49 \text{ ‰}$ ).  
6  
7

## 8 Discussion

### 9 *Origin of graphite morphologies*

10  
11  
12  
13  
14  
15  
16 The variation in the morphology of minerals is related to factors  
17 influencing the growth forms. The theoretical morphology of a mineral, inferred  
18 from its structure, can be used as a reference to evaluate the influence of the  
19 different factors that affect its morphology in a certain setting. In the case of  
20 graphite, the structure is defined by layers of carbon atoms arranged parallel to  
21 the (0001) plane in a hexagonal crystalline lattice, ABAB stacking of aromatic  
22 planes (a rhomboedral polytype, ABCABC stacking, exists as well but is very  
23 minor). Within these layers, strong covalent bonds exist. However, weak van  
24 der Waals forces keep the carbon layers together. The characteristics of this  
25 structure determine that (0001) surface exclusively cuts weak bonds. Therefore,  
26 this is a low attachment energy surface. By contrast, surfaces in the c-axis zone  
27 cut strong bonds and consequently have much higher attachment energies. It is  
28 well known that a direct relationship exists between the attachment energy of a  
29 surface and its growth rate, since the higher the attachment energy the faster  
30 the growth units attach onto it. Thus, any surface in the c-axis zone will grow  
31 much faster than the (0001) surface. Therefore, the expected habit for graphite  
32 crystals will be dominated by (0001) faces, whereas faces in the c-axis zone will  
33 have a very limited development, with the crystals showing a platy morphology.  
34  
35  
36  
37  
38  
39  
40  
41  
42  
43  
44  
45  
46

47 Factors that can affect crystal growth must be considered in the  
48 interpretation of those graphite crystals showing morphologies that differ  
49 significantly from the theoretically expected one. The variation of graphite  
50 morphology can be attributed to (1) changes in the carbonaceous precursor, (2)  
51 the effect of elements other than carbon present in the environment, and (3)  
52 changes in the carbon content of the fluid. Thus, Mostefaoui et al. (2005)  
53 ascribed the various morphologies found in chondrites to different  
54 carbonaceous precursors. Such an assumption could be applied essentially to  
55 graphite in metamorphic rocks formed by graphitization of carbonaceous  
56  
57  
58  
59  
60  
61  
62  
63  
64  
65

1  
2  
3  
4 precursors in situ. However, graphite in metamorphic rocks occurs exclusively  
5 as flakes. On the other hand, it has been reported that in synthetic systems (i.e.  
6 cast irons) some elements (especially magnesium) promote the development of  
7 spherulitic graphite (Double and Hellowell 1995; Östberg 2006). This influence  
8 can be disregarded in natural (geological) systems because the usual  
9 concentrations of such elements in most rocks would lead spherulitic graphite to  
10 be the most common morphology, and this does not actually occur. Thus, for  
11 fluid-deposited graphite occurrences, changes in the carbon content of the fluid  
12 (supersaturation) appear to be the most likely factor controlling the different  
13 graphite morphologies. In particular, unusually high supersaturation is required  
14 for graphite to be precipitated from moderate-temperature fluids (Pasteris  
15 1999), such as those responsible for the Borrowdale mineralization (Luque et al.  
16 2009). High carbon concentrations also seem to play a key role in the  
17 development of graphite spherulites in carbonatite rocks. Spherulitic graphite in  
18 carbonatites, however, does not precipitate from a C-O-H fluid, but it crystallizes  
19 directly from the carbon-rich magma (Doroshkevich et al. 2007).  
20  
21  
22  
23  
24  
25  
26  
27  
28  
29  
30

31 According to classical nucleation theory (Walton 1969), the number of  
32 critical nuclei that form in a system per unit time is an exponential function of the  
33 square of supersaturation. This explains why a large number of crystals reach a  
34 small size when nucleation occurs under high supersaturation conditions, while  
35 few large crystals are the result of nucleation under low supersaturation  
36 (Sunagawa 1987, 2005). Moreover, the formation of aggregates is also  
37 characteristic of crystallization from highly supersaturated fluids. The decrease  
38 in supersaturation during growth results in an evolution from cryptocrystalline  
39 and spherulitic aggregates to polyhedral crystals. If heterogeneous nucleation is  
40 considered and it occurs freely over any surface, various textures of  
41 polycrystalline aggregates will appear through geometrical selection.  
42 Spherulites will be formed on minute, nearly spherical grains during the early  
43 stages of nucleation, whereas cryptocrystalline aggregates displaying banding  
44 parallel to the substrate surface will nucleate and grow over uneven substrate  
45 surfaces (colloform aggregates). Lower supersaturation favours the formation of  
46 polyhedral morphologies mainly by spiral growth (Fig. 6).  
47  
48  
49  
50  
51  
52  
53  
54  
55  
56  
57

58 At high supersaturation conditions the solid-fluid interface becomes  
59 rough and crystal growth occurs by an adhesive or continuous mechanism.  
60  
61  
62  
63  
64  
65

1  
2  
3  
4 Under these conditions, growth is controlled by volume diffusion (Sunagawa  
5 1987) and the resulting morphologies are much more elongated than those  
6 expected at lower supersaturation. If such elongate crystals grow radially  
7 around a minute nucleus, a spherulitic aggregate of acicular crystals will  
8 appear. In natural spherical graphite it has been shown that these spheres  
9 consist of an internal radial arrangement and a thin surface shell with concentric  
10 texture (see Jaszczak 1995). Such textures have been interpreted as the result  
11 of a cone-helix growth mechanism from a common centre (Double and  
12 Hellawell 1974), which is the likely explanation of the origin of graphite  
13 spherulites in the Borrowdale deposit. In other cases, for example in marbles  
14 from Pargas (Finland), the surfaces of these spheres show outlines of individual  
15 graphite crystals with their basal planes lying parallel to the surface. These  
16 spheres are very similar to those found disseminated in the volcanic rocks of  
17 the Borrowdale deposit (compare figures 3a of this paper and 6-11 in Jaszczak  
18 1995). This arrangement of the basal planes of graphite parallel to the substrate  
19 surface could also be responsible for the development of the ring-like textures  
20 observed (Fig. 2c).  
21  
22  
23  
24  
25  
26  
27  
28  
29  
30  
31  
32

33 Dish-like morphologies detected by SEM (Fig. 3f) are reported for the first  
34 time in this paper and they can be interpreted on the basis of structural  
35 considerations. As explained above, the (0001) surface is a low attachment  
36 energy surface while surfaces in the c-axis zone have higher attachment  
37 energies. Consequently, the growth units approaching faces in the c-axis zone  
38 attach onto them much more rapidly than onto (0001) face. Those faces that  
39 grow faster tend to disappear along the growth process. Moreover, when  
40 differences between the growth rates of faces in the same zone are at a  
41 minimum, curved surfaces or edges will develop. In addition, there is also a  
42 relationship between the surface energy of a face and its growth mechanism.  
43 Faces with high attachment energy values tend to be rough and grow by an  
44 adhesive or continuous mechanism. For dish-like graphite morphologies in the  
45 Borrowdale deposit, (0001) faces may have grown by two-dimensional  
46 nucleation, as they appear relatively flat and well developed, whereas those  
47 faces in the c-axis zone must have grown by a continuous mechanism,  
48 appearing as curved ledges (Fig. 3f).  
49  
50  
51  
52  
53  
54  
55  
56  
57  
58  
59  
60  
61  
62  
63  
64  
65

1  
2  
3  
4 Colloform aggregates of graphite were developed over irregular substrate  
5 surfaces starting from minute crystals of random orientation. After one layer is  
6 completed by intermittent growth, repetition of the process will develop the  
7 colloform texture. The interruption and resumption of growth inevitably occur in  
8 a system where there is an imbalance between the diffusion rate and the growth  
9 rate and a critical value such as the energy barrier is involved (Sunagawa  
10 2005). During the early stage of growth, the particle size is small and there is a  
11 high density of nuclei resulting in cryptocrystalline aggregates displaying  
12 banded textures (colloform) parallel to the substrate surface (Figs. 2c and 5).  
13  
14  
15  
16  
17  
18

19 Finally, the most common morphology of graphite crystals (i.e. flaky) from  
20 the Borrowdale deposit would be developed under lower supersaturation  
21 conditions by spiral growth (Fig. 6). Each layer of the graphite structure can be  
22 considered as a two-dimensional sheet to which atoms can be added more  
23 easily in the in-plane directions than along the stacking direction, that is, the c-  
24 axis (normal to the layers). So, as expected from its structure, flakes will be the  
25 dominant morphology for graphite crystals in any natural system (both in  
26 metamorphic and fluid-deposited occurrences; Luque et al. 1998), and any  
27 other morphology would result from particular conditions during nucleation and  
28 growth. Textural relationships in the composite nodules from the Borrowdale  
29 deposit support the conclusion that flaky graphite crystallized later than those  
30 morphologies that formed under high supersaturation conditions  
31 (cryptocrystalline or spherulitic graphite; Figs. 2b, 2d, and 3b).  
32  
33  
34  
35  
36  
37  
38  
39  
40  
41  
42

### 43 ***Structural features of graphite morphologies***

44  
45  
46 According to Raman data, graphite from the Borrowdale deposit is mainly  
47 well-ordered. This is an unexpected feature considering that it was formed at  
48 relatively low temperature (~500 °C; Luque et al. 2009). Under the same  
49 analytical conditions, metamorphic graphite formed at equivalent temperatures  
50 (i.e. greenschist to epidote-amphibolite facies) distinctively shows a lower  
51 degree of order (R1 ratio ranging from 0.30 to 0.50, and average R2 close to  
52 0.45; Beyssac et al. 2002) than that estimated in this study of the Borrowdale  
53 deposit. Compared with metamorphic graphite, the R1 and R2 ratios of the  
54 Raman spectra for the Borrowdale graphite (except for colloform graphite  
55  
56  
57  
58  
59  
60  
61  
62  
63  
64  
65

1  
2  
3  
4 surrounding silicate or sulphide grains in the volcanic host rock) are in the range  
5 for graphite occurring at high grade metamorphic conditions, from upper  
6 amphibolite to granulite facies rocks (Pasteris and Wopenka 1991; Wopenka  
7 and Pasteris 1993; Beyssac et al. 2002). Thus, the Borrowdale deposit  
8 represents the first example of fully ordered graphite in a large graphite  
9 occurrence precipitated from fluids at moderate temperature. The reasons for  
10 such an anomalous crystallinity are discussed in detail in a previous paper  
11 (Luque et al. 2009) and can be summarized as: (1) the different mechanism of  
12 formation for fluid-deposited graphite compared with metamorphic graphite, the  
13 latter being the progressive transformation in situ of a carbonaceous precursor,  
14 (2) the stability field for fully ordered graphite+fluid in the C-O-H system is larger  
15 than that for poorly ordered graphite even at relatively low temperatures, (3) the  
16 heterogeneous nucleation mechanism operating during graphite deposition that  
17 reduced the energy barrier for graphite precipitation from the fluid, and (4) the  
18 fluids responsible for the Borrowdale mineralization had the very high initial  
19 concentration of carbon required for the precipitation of graphite from such  
20 moderate temperature fluids.  
21  
22  
23  
24  
25  
26  
27  
28  
29  
30  
31  
32

33 Considering the overall high crystallinity of graphite in the deposit, an  
34 explanation of the lower crystallinity displayed by the cryptocrystalline graphite  
35 in the colloform textures around pyrite and silicate grains within the volcanic  
36 host rock is required. Colloform graphite around pyrite shows the lowest  
37 crystallinity, with average in-plane crystallite sizes ranging from 150 to 300 Å.  
38 The catalytic effect of certain compounds on the precipitation of graphite,  
39 particularly sulphides (pyrrhotite, stibnite), is well known (Jedwab and Boulegue  
40 1984; Duke and Rumble 1986). Silicates also have been proposed as catalytic  
41 agents during the graphitization of carbonaceous matter through metamorphism  
42 (Grew 1974). So, it is likely that the increased rate of graphite precipitation  
43 caused by these catalysts induced some kind of disorder in the graphite  
44 structure. However, it is worth noting that colloform graphite around quartz in  
45 composite nodules within the mineralized bodies and colloform graphite around  
46 silicates in the volcanic host rocks have contrasting crystallinities. Colloform  
47 graphite around quartz has  $L_a$  values in excess of 2000 Å, whilst colloform  
48 graphite around silicates in the volcanic host rocks has  $L_a=200-300$  Å. Thus, it  
49 seems likely that ferromagnesian minerals within the host rock caused a similar  
50  
51  
52  
53  
54  
55  
56  
57  
58  
59  
60  
61  
62  
63  
64  
65

1  
2  
3  
4 effect to that of pyrite, whereas quartz does not appear to influence any  
5 structural disorder in the precipitated graphite.  
6

7 As with cryptocrystalline graphite, graphite spherulites also developed  
8 under high supersaturation conditions. Raman parameters measured on  
9 spherulitic graphite within nodules from the mineralized bodies indicate a high  
10 degree of ordering, similar to that found in graphite from high-grade  
11 metamorphic rocks, with  $L_a$  larger than of 2000 Å. In addition, graphite  
12 spherulites in the chlorite-graphite veins also have large  $L_a$  crystallite sizes  
13 (>1000 Å). Previous Raman data on graphite spherulites both in synthetic  
14 systems (cast irons) and natural occurrences (chondrite meteorites and  
15 carbonatites) point to poorly crystalline materials. Cooper et al. (2003) reported  
16 Raman spectra from spherulitic graphite in cast irons showing intense D1 and  
17 D2 peaks that reveal low crystallinity. Mostefaoui et al. (2000) found spherulitic  
18 graphite in primitive chondrites with  $L_a$  between 30 and 40 Å. Similarly,  
19 Doroshkevich et al. (2007) reported graphite spherulites in carbonatites with R1  
20 in the range 0.35-0.84. The large difference in crystallinity between graphite  
21 spherulites in cast irons and carbonatites, and those found in Borrowdale can  
22 be interpreted as a consequence resulting from an unlikely analytical procedure.  
23 In both the cast irons and carbonatites, the Raman measurements were done  
24 on polished surfaces and the polishing process appears to be the cause of such  
25 a low crystallinity. The Raman spectra on graphite spherulites in chondrites  
26 were obtained over unpolished surfaces, so a different argument should be  
27 invoked to explain its low crystallinity. Graphite in chondrites results from  
28 heating of carbonaceous precursors at high temperatures (> 1000 °C) for a very  
29 short period of time, with no pressure contribution (Mostefaoui et al. 2000).  
30 Such conditions are similar to those of experimental graphitization (Beny-  
31 Bassez and Rouzaud 1985) in which the products displayed Raman spectra  
32 corresponding to poorly crystalline graphite. Thus, the very different crystallinity  
33 of graphite spherulites in chondrites compared with those from Borrowdale  
34 should be attributed to their contrasting mechanisms of formation.  
35  
36  
37  
38  
39  
40  
41  
42  
43  
44  
45  
46  
47  
48  
49  
50  
51  
52  
53  
54  
55  
56  
57  
58  
59  
60  
61  
62  
63  
64  
65

1  
2  
3  
4 ***Significance of the carbon isotope ratios***  
5  
6

7 In a first approach, stable carbon isotope ratios in graphite provide  
8 information about the origin of the carbon. For fluid-deposited graphite, the  
9 possible sources of carbon are (a) devolatilization of carbonaceous metapelites,  
10 (b) decarbonation of carbonate rocks, and (c) mantle-derived carbon (Luque et  
11 al. 1998). Each source has carbon isotope ratios falling within characteristic  
12 ranges. The total range of  $\delta^{13}\text{C}$  values for organic matter (both living and dead)  
13 is from about -40 to +6 ‰, with an average  $\delta^{13}\text{C}$  value of -25 ‰; that is, organic  
14 materials are isotopically light (Weis et al. 1981). Marine carbonates of  
15 Cambrian to Tertiary age, on the other hand, have heavier  $\delta^{13}\text{C}$  values which lie  
16 within  $\pm 2$  units of 0 ‰. The isotopic compositions of diamonds and mid-oceanic  
17 ridge basalts (MORB) indicate that carbon from the mantle is significantly  
18 heavier ( $\delta^{13}\text{C} = -7$  ‰) than biogenically derived carbon (Crespo et al. 2006).  
19  
20  
21  
22  
23  
24  
25  
26  
27

28 The interpretation of the carbon isotopic signature in terms of the carbon  
29 source is complicated by fractionation effects related to the thermal history of  
30 the rock or to carbon-exchange between graphite and other carbon-bearing  
31 species, such as an isotopically heavier carbonate (which in turn is also  
32 governed by temperature). In the fractionation that occurs between two phases,  
33 the more oxidized species of the pair becomes relatively enriched in the heavier  
34 isotope, i.e.  $^{13}\text{C}$ . In the maturation of organic matter, fractionation occurs  
35 between organic residues and their evolved gas species. For a fluid co-existing  
36 with the FQM buffer, the fluid becomes richer in the oxidized species ( $\text{CO}_2$ ) with  
37 increasing temperature (Frost 1979). Thus, at low temperature and under low  
38  $f\text{O}_2$  conditions, co-existing  $\text{CH}_4$  becomes depleted in  $^{13}\text{C}$ , giving the gas an  
39 isotopically lighter signature and the residual carbonaceous matter a heavier  
40 one (Bottinga 1969). At relatively high  $f\text{O}_2$  the carbon-bearing species resulting  
41 from devolatilization of carbonaceous matter would be an isotopically light  $\text{CO}_2$ ,  
42 but heavier than the residual carbonaceous matter. The decarbonation  
43 reactions of carbonate minerals result in a  $^{13}\text{C}$ -enriched  $\text{CO}_2$  phase.  
44 Incorporation of such  $\text{CO}_2$  into aqueous fluids would lead to the precipitation of  
45 isotopically heavy graphite. Finally, the possibility of mixing between different  
46 carbon reservoirs before or while graphite precipitated from the fluid should be  
47  
48  
49  
50  
51  
52  
53  
54  
55  
56  
57  
58  
59  
60  
61  
62  
63  
64  
65

1  
2  
3  
4 also considered when interpreting the carbon isotopic signature of fluid-  
5 deposited graphite (see Luque et al. 1998).  
6

7 The light isotopic signatures of the different morphologies of graphite  
8 from the Borrowdale deposit suggest that the carbon was derived from a  
9 biogenic source. This is in good agreement with the geological and geochemical  
10 evidence of assimilation of Skiddaw Group metapelites by the volcanic host  
11 rocks, and with the presence of zones within the metapelites that have been  
12 depleted in carbon and other elements during hydrothermal alteration (e.g. the  
13 Crummock Water zone, Fig. 1; Cooper et al. 1988). As previously mentioned,  
14 the bulk carbon isotopic analyses of Skiddaw metapelites yielded values close  
15 to  $\delta^{13}\text{C} = -28.5 \text{ ‰}$ . Considering the solidus temperature of andesite magmas,  
16 the assimilation of the Skiddaw metapelites should occur at temperatures close  
17 to 1100 °C. At such temperature the released carbon species is  $\text{CO}_2$ , and the  
18 fractionation factor C- $\text{CO}_2$  is about 5.5 ‰ (Scheele and Hoefs 1992). Thus, the  
19  $\delta^{13}\text{C}$  value for the  $\text{CO}_2$  at the assimilation temperature was close to -23 ‰. At  
20 the temperature estimated for graphite precipitation (480-500 °C; Luque et al.  
21 2008), the fractionation factors for  $\text{CO}_2$ -C would be close to 10.5 ‰ (Bottinga  
22 1969). This means that the graphite precipitated from this  $\text{CO}_2$ -rich fluid should  
23 have an isotopic signature close to -33.5 ‰.  
24  
25  
26  
27  
28  
29  
30  
31  
32  
33  
34  
35

36 Fluid inclusion data in the Borrowdale deposit (Ortega et al. 2008, Luque  
37 et al. 2008) have shown that fluids involved in the mineralizing process had  
38 average compositions of 0.65 mol fraction  $\text{H}_2\text{O}$  and  $\text{XCO}_2/(\text{XCO}_2+\text{XCH}_4)= 0.69$   
39 in the main stage of graphite precipitation. Later, the fluids evolved towards 0.93  
40 mol fraction  $\text{H}_2\text{O}$  and  $\text{XCO}_2/(\text{XCO}_2+\text{XCH}_4)= 0$ , with  $\text{CH}_4$  being the only carbonic  
41 species in the fluid in the final stages of fluid circulation. The graphite-  
42 mineralizing fluid would be a vapour-like supercritical phase at the beginning of  
43 the graphite precipitation, evolving to a liquid-rich fluid as the deposition  
44 proceeded. The conspicuous relationship between epidote and graphite in the  
45 breccia pipe-like bodies strongly suggests that the graphite precipitation started  
46 following the reaction  $\text{CO}_2 \rightarrow \text{C} + \text{O}_2$ . Since the average  $\text{XCO}_2$  in the early fluid  
47 is 0.24 and epidote is not stable for  $\text{XCO}_2 > 0.2$  (Liou 1993), epidote  
48 crystallization was likely triggered by the consumption of  $\text{CO}_2$  in the reaction of  
49 graphite precipitation. The earlier morphologies (colloform) crystallizing in the  
50 pipe-like bodies display lighter signatures ( $\delta^{13}\text{C} = -33.7 \text{ ‰}$ ) than flaky graphite  
51  
52  
53  
54  
55  
56  
57  
58  
59  
60  
61  
62  
63  
64  
65

1  
2  
3  
4 ( $\delta^{13}\text{C} = -30.2 \text{ ‰}$ ) that formed somewhat later. The values for cryptocrystalline  
5 graphite forming colloform textures in the composite nodules has therefore  
6 isotopic signatures similar to that of graphite crystallizing from  $\text{CO}_2$  in the fluid  
7 with an initial  $\delta^{13}\text{C}$  around  $-23 \text{ ‰}$ . Flaky graphite is on average  $3.5 \text{ ‰}$  heavier  
8 than colloform graphite within the main mineralized bodies, and this can be  
9 ascribed to  $\text{CO}_2$  consumption in the fluid. It has been documented that changes  
10 in the  $\text{CO}_2/\text{CH}_4$  ratio in the fluid may result in relatively large isotopic shifts.  
11 Such variations in the  $\text{CO}_2/\text{CH}_4$  ratio can be also influenced by changes in the  
12  $\text{XH}_2\text{O}$ , for example, by hydration reactions occurring simultaneously with  
13 graphite deposition (Duke and Rumble 1986).  
14

15  
16 Fluid inclusion data reveal a progressive enrichment in water as graphite  
17 mineralization proceeded, pointing to the involvement of water-generating  
18 reactions during graphite deposition: (1)  $\text{CH}_4 + \text{O}_2 \rightarrow \text{C} + 2\text{H}_2\text{O}$  or (2)  $\text{CH}_4 +$   
19  $\text{CO}_2 \rightarrow 2\text{C} + 2\text{H}_2\text{O}$  (or both). The reaction between  $\text{CH}_4$  and  $\text{CO}_2$  to form  
20 graphite is kinetically very sluggish, so reaction (1) seems to be more likely to  
21 account for graphite deposition in a later stage of the mineralizing event. The  
22 simultaneous consumption of  $\text{CH}_4$  and water enrichment in the fluid drove its  
23 composition along the graphite saturation curve towards the  $\text{CO}_2$ -rich side,  
24 resulting in an isotopic shift towards lighter  $\delta^{13}\text{C}$  values in the precipitated  
25 graphite (Fig. 7). In this way, the isotopic signature of vermicular graphite ( $\delta^{13}\text{C}$   
26  $= -34.5 \text{ ‰}$ ) in graphite-chlorite assemblages from fault-fills would be lighter than  
27 that of the earlier formed spherulitic graphite ( $\delta^{13}\text{C} = -30.2 \text{ ‰}$ ). This suggests,  
28 though does not prove, that graphite-chlorite veins represent a slightly later  
29 mineralizing phase involving deposition from fluids in which the dominant  
30 carbonic species became  $\text{CH}_4$ . The variations in the  $\delta^{13}\text{C}$  values between the  
31 different graphite morphologies (both in the pipes and in the graphite-chlorite  
32 veins) can be explained therefore through a Rayleigh distillation mechanism  
33 from an initial  $\text{CO}_2\text{-CH}_4\text{-H}_2\text{O}$  single fluid promoting graphite precipitation over a  
34 narrow (nearly isothermal) temperature interval. This interpretation is consistent  
35 with the evolution of the composition of the fluid obtained from fluid inclusion  
36 data and agrees with the morphology of the mineralized bodies (pipe-like  
37 breccias) which indicates a rapid, catastrophic mineralizing event.  
38  
39  
40  
41  
42  
43  
44  
45  
46  
47  
48  
49  
50  
51  
52  
53  
54  
55  
56  
57  
58  
59  
60  
61  
62  
63  
64  
65

## Conclusions

Graphite in the Borrowdale (Cumbria, UK) deposit occurs as large masses within mineralized pipe-like bodies, as late graphite-chlorite veins, and disseminated through its andesite and dioritic host rocks. Graphite from Borrowdale shows the greatest variety of crystalline morphologies recognized up to now from a single deposit. In addition to flaky crystals, graphite also occurs as cryptocrystalline aggregates displaying colloform textures (reported for the first time in any graphite deposit worldwide), as spherulitic aggregates, and with dish-like morphologies. Colloform graphite occurs around silicate (both ferromagnesian minerals of the volcanic host rock and quartz within the breccia pipe mineralized body) and sulphide (mainly pyrite in the host rock) substrates. Textural relationships indicate that spherulitic aggregates and colloform textures are earlier than flaky crystals. This sequence of crystallization is related to the precipitation of graphite from fluids with progressively decreasing supersaturation.

With the exception of colloform graphite around silicate and pyrite grains within the host rocks, all graphite morphologies display very high crystallinity, as revealed by their in-plane crystallite sizes. Such high crystallinity is unusual for moderate-temperature fluid-deposited graphite and this has been discussed in detail in a previous paper (Luque et al. 2009). The lower crystallinity of colloform graphite within the host rock is attributed to the structural disorder induced by the catalytic effect of ferromagnesian and sulfide minerals during crystallization.

The light stable carbon isotope ratios of graphite ( $\delta^{13}\text{C} = -34.5$  to  $-30.2\%$ ) are compatible with the assimilation of carbon-bearing metapelites in the Borrowdale Volcanic Group magmas. In the main mineralized breccia pipe-like bodies, the microscale isotopic signatures (with cryptocrystalline graphite being lighter than flaky graphite) are consistent with the composition and evolution of the mineralizing fluids which indicate a progressive loss of  $\text{CO}_2$  (from precipitation of graphite through the reaction  $\text{CO}_2 \rightarrow \text{C} + \text{O}_2$ ). Late graphite-chlorite veins contain isotopically heavier spherulitic graphite than flaky graphite. This agrees with the fact that the fluids, as evidenced from fluid inclusion data, were richer in  $\text{CH}_4$  at this stage of the mineralizing event, resulting in the successive precipitation of isotopically heavier graphite

1  
2  
3  
4 morphologies. The dominant graphite-producing reaction at this stage was  $\text{CH}_4$   
5 +  $\text{O}_2 \rightarrow \text{C} + 2\text{H}_2\text{O}$ . Thus, the isotopic variations of the different graphite  
6 morphologies can be attributed to changes in the speciation of carbon in the  
7 fluids coupled with concomitant changes in the  $\text{XH}_2\text{O}$  during precipitation of  
8 graphite and associated hydrous minerals (mainly epidote and chlorite).  
9  
10  
11  
12  
13

### 14 ***Acknowledgements***

15  
16  
17 Access to the Edinburgh Ion Microprobe Facility through N.E.R.C.  
18 Scientific Services is gratefully acknowledged. We thank John Craven for his  
19 expertise, interest and support. Dr L. Fernández-Díaz is also thanked for helpful  
20 suggestions about the mechanisms of nucleation and growth. Technical  
21 assistance by E. Baldonado (Centro de Microscopía Electrónica Luis Bru, UCM)  
22 during SEM work is also gratefully acknowledged. This paper is a contribution  
23 from project CGL2006-00835 of the Spanish Ministry of Science and Innovation.  
24 David Millward publishes with the permission of the Executive Director, British  
25 Geological Survey (N.E.R.C.). This study was partly funded by INSU DyETI and  
26 ANR JC (GeoCarbons project) to Olivier Beyssac.  
27  
28  
29  
30  
31  
32  
33  
34  
35  
36

### 37 **References**

- 38  
39  
40 Barrenechea JF, Luque FJ, Rodas M, Pasteris JD (1997) Vein-type graphite  
41 mineralization in the Jurassic volcanic rocks of the external zone of the  
42 Betic Cordillera (Southern Spain). *Can Mineral* 35: 1379-1390  
43  
44 Barrenechea JF, Luque, FJ, Ortega L, Rodas M, Millward D, Beyssac O (2008)  
45 Graphite morphologies in the volcanic-hosted deposit at Borrowdale (NW  
46 England, UK): preliminary Raman and SIMS data. *Macla* 9: 91-92  
47  
48 Beny-Bassez C, Rouzaud J-N (1985) Characterization of carbonaceous  
49 materials by correlated electron optical microscopy and Raman  
50 microspectroscopy. *Scanning Electron Microscop* 1985: 119-132  
51  
52 Beyssac O, Goffé B, Chopin C, Rouzaud, J-N (2002) Raman spectra of  
53 carbonaceous materials in metasediments: a new geothermometer. *J*  
54 *metamorphic Geol* 20: 859-871  
55  
56  
57  
58  
59  
60  
61  
62  
63  
64  
65

- 1  
2  
3  
4 Beyssac O, Goffé B, Petitet JP, Froigneux E, Moreau M, Rouzaud, J-N (2003)  
5 On the characterization of disordered and heterogeneous carbonaceous  
6 materials by Raman spectroscopy. *Spectrochim Acta, Part A* 59: 2267-  
7 2276  
8  
9  
10  
11 Bottinga Y (1969) Calculated fractionation factors for carbon and hydrogen  
12 isotope exchange in the system calcite-carbon dioxide-graphite-  
13 methane-hydrogen-water vapor. *Geochim Cosmochim Acta* 33: 49-64  
14  
15 Cooper AH, Rushton AWA, Molyneux SG, Hughes, RA, Moore RM, Webb BC  
16 (1995) The stratigraphy, correlation, provenance and paleogeography of  
17 the Skiddaw Group (Ordovician) in the English Lake District. *Geol Mag*  
18 132: 185-211  
19  
20  
21  
22 Cooper AH, Fortey NJ, Hughes RA, Molyneux, SG, Moore RM, Rushton, AWA,  
23 Stone P, Allen PM, Cooper DC, Evans JA, Hirons SR, Webb, BC (2004)  
24 The Skiddaw Group of the English Lake District. *Memoir of the British*  
25 *Geological Survey*. London: HMSO  
26  
27  
28  
29 Cooper CA, Elliot R, Young RJ (2003) Investigation of the graphitic  
30 microstructure in flake and spheroidal cast irons using Raman  
31 spectroscopy. *J Mater Sci* 38: 795-802  
32  
33  
34  
35 Cooper D C, Lee MK, Fortey NJ, Cooper AH, Rundle CC, Webb BC, Allen PM  
36 (1988) The Crummock Water aureole: a zone of metasomatism and  
37 source of ore metals in the English Lake District. *J Geol Soc, London*  
38 145: 523-540  
39  
40  
41  
42 Coplen TB, Brand WA, Gehre M, Gröning M, Meijer HAJ, Toman B,  
43 Verkouteren RM (2006) New guidelines for  $\delta^{13}\text{C}$  measurements. *Anal*  
44 *Chem* 78: 2439-2441  
45  
46  
47 Crespo E, Luque J, Rodas M, Wada H, Gervilla F (2006) Graphite-sulfide  
48 deposits in Ronda and Beni Bousera peridotites (Spain and Morocco)  
49 and the origin of carbon in mantle-derived rocks. *Gondwana Res* 9, 279-  
50 290  
51  
52  
53  
54 Doroshkevich AG, Wall F, Ripp, GS (2007) Magmatic graphite in dolomite  
55 carbonatite at Pogranichnoe, North Transbaikalia, Russia. *Contrib*  
56 *Mineral Petrol* 153: 339-353  
57  
58  
59  
60  
61  
62  
63  
64  
65

- 1  
2  
3  
4 Double DD, Hellawell A (1974) Cone-helix growth forms of graphite. *Acta Metall*  
5 22: 481-487  
6  
7 Double DD, Hellawell A (1995) The nucleation and growth of graphite: the  
8 modification of cast iron. *Acta Metall Mater* 43: 2435-2442  
9  
10 Duke EF, Rumble D (1986) Textural and isotopic variations in graphite from  
11 plutonic rocks, South-Central New Hampshire. *Contrib Mineral Petrol* 93:  
12 409-419  
13  
14  
15 El Goresy A, Zinner E, Pellas P, Caillet C (2005) A menagerie of graphite  
16 morphologies in the Acapulco meteorite with diverse carbon and nitrogen  
17 isotopic signatures: Implications for the evolution history of acapulcoite  
18 meteorites. *Geochim Cosmochim Acta* 69: 4535-4556  
19  
20  
21  
22 Fitton JG (1972) The genetic significance of almandine-pyrope phenocrysts in  
23 the calc-alkaline Borrowdale Volcanic Group, northern England. *Contrib*  
24 *Mineral Petrol* 36: 231-248  
25  
26  
27 Frost BR (1979) Mineral equilibria involving mixed-volatiles in a C-O-H fluid  
28 phase: the stabilities of graphite and siderite. *Am J Sci* 279: 1033-1059  
29  
30  
31 Gellatly DC (1966) Graphite in natural and experimental carbonate systems.  
32 *Miner Mag* 35: 963-970  
33  
34  
35 Gogotsi Y, Libera JA, Kalashnikov N, Yoshimura M (2000) Graphite polyhedral  
36 crystals. *Science* 290: 317-320  
37  
38  
39 Grew ES (1974) Carbonaceous materials in some metamorphic rocks of New  
40 England and other areas. *J Geol* 82: 50-73  
41  
42 Jaszczak JA (1995) Graphite: Flat, Fibrous and Spherical. In Mendenhall GD  
43 (ed) *Mesomolecules: From Molecules to Materials*. Chapman and Hall,  
44 London  
45  
46  
47 Jaszczak JA, Robinson GW, Dimovski S, Gogotsi Y (2003) Naturally occurring  
48 graphite cones. *Carbon* 41: 2085-2092  
49  
50  
51 Jaszczak JA, Dimovski S, Hackney SA, Robinson, GW, Bosio P, Gogotsi Y  
52 (2007) Micro- and nanoscale graphite cones and tubes from Hackman  
53 Valley, Kola Peninsula, Russia. *Can Mineral* 45: 379-389  
54  
55  
56 Jedwab J, Boulegue J (1984) Graphite crystals in hydrothermal vents. *Nature*,  
57 310: 41-43  
58  
59  
60 Katz MB (1987) Graphite deposits of Sri Lanka: a consequence of granulite  
61 facies metamorphism. *Miner Deposita*, 22, 18-25  
62  
63  
64  
65

- 1  
2  
3  
4 Kavanagh A, Schlogl R (1988) The morphology of some natural and synthetic  
5 graphites. Carbon 26: 23-32  
6
- 7 Kvasnitsa VN, Yatsenko VG, Jaszczak JA (1999) Disclinations in unusual  
8 graphite crystals from anorthosites of Ukraine. Can Mineral 37: 951-960  
9
- 10 Kwiecinska B (1980) Mineralogy of natural graphites. Polska Akad Nauk, Prace  
11 Mineral, 67: 5-79  
12
- 13  
14 Lespade P, Al-Jishi R, Dresselhaus, MS (1982) Model for Raman scattering  
15 from incompletely graphitized carbons. Carbon 20: 427-431  
16
- 17 Liou JG (1993) Stabilities of natural epidotes In Hock V and Koller F (eds) Proc  
18 125 Jahre Kappenwand Symposium: 7-16  
19
- 20  
21 Lowry D, Boyce AJ, Pattrick RAD, Fallick AE, Stanley CJ (1991) A sulphur  
22 isotopic investigation of the potential sulphur sources for Lower  
23 Palaeozoic-hosted vein mineralization in the English Lake District. J Geol  
24 Soc, London 148, 993-1004  
25
- 26  
27 Luque FJ, Pasteris JD, Wopenka B, Rodas M, Barrenechea JF (1998) Natural  
28 fluid-deposited graphite: mineralogical characteristics and mechanisms of  
29 formation. Am J Sci 298: 471-498  
30
- 31  
32  
33 Luque FJ, Ortega L, Barrenechea JF, Millward D, Beyssac O, Huizenga, J-M  
34 (2009) Deposition of highly crystalline graphite from moderate-  
35 temperature fluids. Geology: in press  
36
- 37  
38 McConnell BJ, Menuge JF, Hertogen J (2002) Andesite petrogenesis in the  
39 Ordovician Borrowdale Volcanic Group of the English Lake District by  
40 fractionation, assimilation and mixing. J Geol Soc, London 159: 417-424  
41
- 42  
43 Millward D (2004) The Caradoc volcanoes of the English Lake District. Proc  
44 Yorkshire Geol Soc 55: 73-105  
45
- 46  
47 Mostefaoui S, Perron C, Zinner E, Sagon, G (2000) Metal-associated carbon in  
48 primitive chondrites: Structure, isotopic composition, and origin. Geochim  
49 Cosmochim Acta 64: 1945-1964  
50
- 51  
52 Mostefaoui S, Zinner E, Hoppe P, Stadermann FJ, El Goresy, A. (2005) In situ  
53 survey of graphite in unequilibrated chondrites: Morphologies, C, N, O  
54 and H isotopic ratios. Meteoritics Planet Sci 40: 721-743  
55
- 56  
57 Ortega L, Luque J, Barrenechea JF, Millward D, Beyssac O, Huizenga, J-M,  
58 Rodas, M (2008) Fluid composition and reactions of graphite precipitation  
59  
60  
61  
62  
63  
64  
65

1  
2  
3  
4 in the volcanic-hosted deposit at Borrowdale (NW England): evidence  
5 from fluid inclusions. *Macla* 9: 177-178  
6

7 Östberg G (2006) Perspectives on research on the formation of nodular  
8 graphite in cast iron. *Mater Design* 27: 1007-1015  
9

10 Pasteris JD (1989) In situ analysis in geological thin-sections by Laser Raman  
11 Microprobe Spectroscopy: a cautionary note. *App Spectr* 43: 567-570  
12

13 Pasteris JD (1999) Causes of the uniformly high crystallinity of graphite in large  
14 epigenetic deposits. *J metamorphic Geol* 17: 779-787  
15

16 Pasteris JD, Wopenka B (1991) Raman spectra of graphite as indicators of  
17 degree of metamorphism. *Can Mineral* 29: 1-9  
18

19 Pimenta MA, Dresselhaus G, Dresselhaus MS, Cancado LG, Jorio A, Saito R  
20 (2007) Studying disorder in graphite-based systems by Raman  
21 spectroscopy. *Phys Chem Chem Phys* 9: 1276-1291  
22

23 Reich S, Thomsen C (2004) Raman spectroscopy of graphite. *Phil Trans Royal*  
24 *Soc London, A* 362: 2271-2288  
25

26 Rumble D, Ferry JM, Hoering TC, Boucot, AJ (1982) Fluid flow during  
27 metamorphism at the Beaver Brook fossil locality, New Hampshire. *Am J*  
28 *Sci* 282: 886-919  
29

30 Scheele N, Hoefs J (1992) Carbon isotope fractionation between calcite,  
31 graphite and CO<sub>2</sub>: an experimental study. *Contrib Mineral Petrol* 112: 35-  
32 45  
33

34 Strens RGJ (1965) The graphite deposit of Seathwaite in Borrowdale,  
35 Cumberland. *Geol Mag* 102: 393-406  
36

37 Sunagawa I (1987) Morphology of Minerals. In Sunagawa I (ed) *Morphology of*  
38 *Crystals, Part B*. Terra Scientific, Tokyo. pp. 509-587  
39

40 Sunagawa I (2005) *Crystals: Growth, Morphology and Perfection*. Cambridge  
41 University Press, Cambridge  
42

43 Tan PH, Dimovski S, Gogotsi Y (2004) Raman scattering of non-planar  
44 graphite: arched edges, polyhedral crystals, whiskers and cones. *Phil*  
45 *Trans R Soc London, A* 362: 2289-2310  
46

47 Walton AG (1969) Nucleation in liquids and solutions. In Zettlemoyer AC (ed)  
48 *Nucleation*. Marcel Dekker, New York  
49

50  
51  
52  
53  
54  
55  
56  
57  
58  
59  
60  
61  
62  
63  
64  
65

1  
2  
3  
4  
5  
6  
7  
8  
9  
10  
11  
12  
13  
14  
15  
16  
17  
18  
19  
20  
21  
22  
23  
24  
25  
26  
27  
28  
29  
30  
31  
32  
33  
34  
35  
36  
37  
38  
39  
40  
41  
42  
43  
44  
45  
46  
47  
48  
49  
50  
51  
52  
53  
54  
55  
56  
57  
58  
59  
60  
61  
62  
63  
64  
65

Ward JC (1876) The geology of the northern part of the English Lake District.  
Memoir of the Geological Survey of Great Britain. Quarter Sheet 101SE  
(England & Wales Sheet 29, Keswick)

Weis PL, Friedman I, Gleason, JP (1981) The origin of epigenetic graphite:  
evidence from isotopes. *Geochim Cosmochim Acta* 45: 2325-2332

Wopenka B, Pasteris JD (1993) Structural characterization of kerogens to  
granulite-facies graphite: Applicability of Raman microprobe  
spectroscopy. *Am Mineral* 78: 533-557

1  
2  
3  
4  
5  
6  
7  
8  
9  
10  
11  
12  
13  
14  
15  
16  
17  
18  
19  
20  
21  
22  
23  
24  
25  
26  
27  
28  
29  
30  
31  
32  
33  
34  
35  
36  
37  
38  
39  
40  
41  
42  
43  
44  
45  
46  
47  
48  
49  
50  
51  
52  
53  
54  
55  
56  
57  
58  
59  
60  
61  
62  
63  
64  
65

## CAPTIONS OF FIGURES

**Fig. 1** Simplified geological map of the English Lake District (UK) locating the Borrowdale graphite deposit at Seathwaite. The bleached and metasomatically altered zone with the Skiddaw Group at Crummock Water (CW) is also shown

**Fig. 2** Morphologies of graphite crystals and aggregates from the Borrowdale deposit. a) Section of a hand sample showing the rounded to elliptical section of the graphite nodules within the altered andesite host rock. Scale is in centimeters. Photos b) to f) are reflected light photomicrographs (one polarizer). b) Detail of the contact (dashed line) between flaky graphite (FG) and cryptocrystalline graphite (CG) in a composite nodule. c) Large arrow points to an encapsulated quartz fragment (dark grey) with small graphite spherulites inside (light grey) embedded in cryptocrystalline (colloform) graphite; note the small graphite ring at the upper left corner of the photo (small arrow). d) Rounded patch of cryptocrystalline graphite (CG) within flaky graphite (FG). e) Colloform graphite (light grey) within the volcanic host rock; note reflectivity zoning parallel to the margins of the graphite aggregate. f) Colloform graphite (light grey) around pyrite (white)

**Fig. 3** Morphologies of graphite crystals and aggregates from the Borrowdale deposit. a) Scanning electron microscope image of graphite spherulites disseminated within the volcanic host rock. Photos b) to e) are reflected light photomicrographs (one polarizer). b) The arrow points to a graphite spherulite within flaky graphite. c) Aggregate of graphite spherulites within chlorite. d) Curved and tapering graphite flakes intergrown with chlorite. e) Vermicular graphite intergrown with chlorite. f) Scanning electron microscope image of dish-like graphite

**Fig. 4** First-order Raman spectra of the different graphite morphologies from the Borrowdale deposit. a) flaky graphite, b) cryptocrystalline graphite from composite nodules, c) colloform graphite surrounding silicate grains

1  
2  
3  
4 within the volcanic host rock (hr), d) colloform graphite surrounding pyrite  
5 (py) within the volcanic host rock, e) spherulitic graphite included in  
6 encapsulated quartz, f) spherulitic graphite within chlorite (chl)  
7  
8  
9

10  
11 **Fig 5** Reflected light microphotograph (one polarizer) of a composite nodule  
12 showing the  $\delta^{13}\text{C}$  values of cryptocrystalline (colloform) graphite. The  
13 points analyzed by SIMS are indicated by small circles  
14  
15

16  
17 **Fig. 6** Schematic diagram depicting the relationship between supersaturation  
18 and growth rate (based on Sunagawa 1987). The type of surface of  
19 aggregates and crystals and the nucleation mechanism prevailing in  
20 each field (in brackets) are shown. The images correspond to the three  
21 main graphite morphologies found in the Borrowdale deposit: 1-  
22 cryptocrystalline, 2- spherulitic, and 3- flaky  
23  
24  
25  
26  
27  
28

29  
30 **Fig. 7** Phase diagram of the C-O-H system at 600 °C and 3.5 kbar showing the  
31 graphite-fluid isotopic fractionation as a function of fluid composition  
32 (modified after Duke and Rumble 1986). Along the graphite saturation  
33 curve, for  $\text{CO}_2$ -rich fluids (like fluid A in the graph),  $\text{CO}_2$ -depletion and/or  
34  $\text{H}_2\text{O}$ -enrichment will result in the precipitation of isotopically heavier  
35 graphite. The first mineralizing fluids in the Borrowdale deposit were  
36 similar in composition to fluid A (Luque et al. 2009). Conversely,  $\text{CH}_4$ -  
37 depletion and/or water-enrichment in  $\text{CH}_4$ -rich fluids (like fluid B) will  
38 cause the precipitation of isotopically lighter graphite. These qualitative  
39 variations of  $\Delta_{\text{graphite-fluid}} = \delta^{13}\text{C}_{\text{graphite}} - \delta^{13}\text{C}_{\text{fluid}}$  are relatively insensitive to the  
40 exact temperature chosen for the system (Duke and Rumble 1986). For  
41 explanation see text  
42  
43  
44  
45  
46  
47  
48  
49  
50  
51  
52  
53  
54  
55  
56  
57  
58  
59  
60  
61  
62  
63  
64  
65

**Table 1** Morphologies and characteristics of graphite from the Borrowdale deposit

	<b>Morphology</b>	<b>Occurrence</b>	<b>Host</b>	<b>Remarks</b>
	Flaky, scaly	Nodules, irregular patches, coatings, disseminations	Altered andesite and diorite	Randomly distributed within nodules and patches (Fig. 2b)
Aggregates	Spherulitic	Patches	Chlorite	Individual size of spherulites ranging from 5-10 $\mu\text{m}$ in diameter (Fig. 3c)
	Cryptocrystalline	Patches, colloform	Altered andesite, flaky graphite (composite nodules)	Masses, bands and "globules" with apparent reflectance zoning (Figs. 2c, 2d, 2e, 2f, 5)
Individual forms	Spherulites	Disseminations	Flaky graphite	5-40 $\mu\text{m}$ in diameter (Fig. 3b)
	Spherulites	Disseminations	Altered andesite	1-5 $\mu\text{m}$ in diameter (Fig. 3a)
	Spherulites	Disseminations	Encapsulated quartz fragments	1-3 $\mu\text{m}$ in diameter (Fig. 2c)
	Rings	Disseminations	Cryptocrystalline graphite, altered andesite	Nucleated on silicate or sulfide grains (Fig. 2c)
	Flakes	Graphite-chlorite intergrowths	Chlorite	Thin curved and tapering crystals (Fig. 3d)
	Vermicular	Graphite-chlorite intergrowths	Chlorite	Randomly distributed within chlorite (Fig. 3e)
	Disks	Disseminations	Altered andesite	20-40 $\mu\text{m}$ in diameter (Fig. 3f)

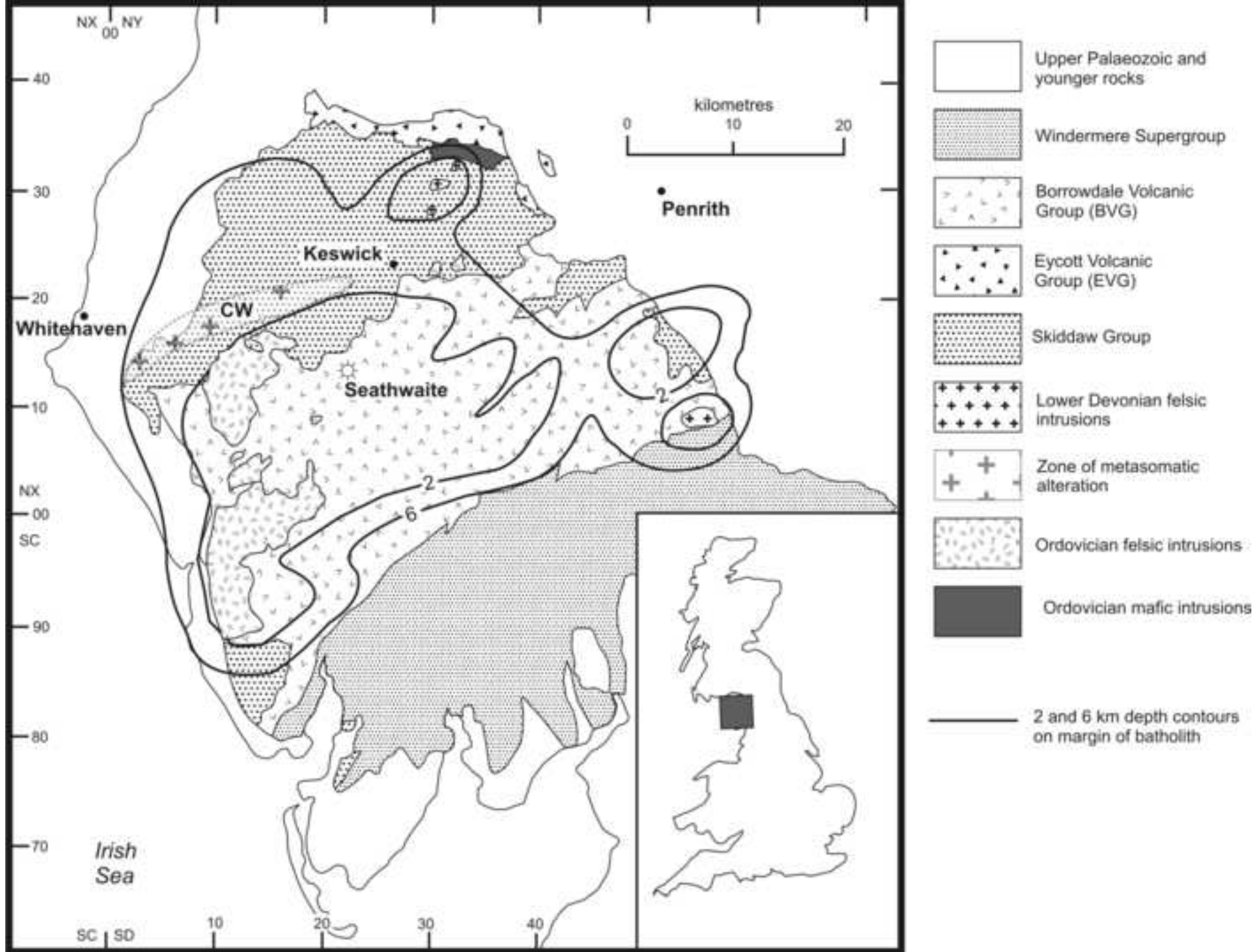
**Table 2** Raman data for the different graphite morphologies

	G position (cm <sup>-1</sup> )	D1 position (cm <sup>-1</sup> )	G FWHM (cm <sup>-1</sup> )	R1	R2		G position (cm <sup>-1</sup> )	D1 position (cm <sup>-1</sup> )	G FWHM (cm <sup>-1</sup> )	R1	R2
<b>Flaky</b>						<b>Colloform (silicate)</b>					
Mean value	1581	1350	20	0.04	0.06	Mean value	1582	1355	27	0.23	0.25
Std dev	1.2	2.5	2.9	0.09	0.09	Std dev	1.7	2.8	2.5	0.09	0.09
Number of analyses	25					Number of analyses	28				
<b>Cryptocrystalline</b>						<b>Colloform (pyrite)</b>					
Mean value	1581	1355	21	0.09	0.05	Mean value	1583	1356	26	0.26	0.28
Std dev	1.3	2.3	1.5	0.02	0.08	Std dev	1.0	2.4	2.2	0.08	0.07
Number of analyses	17					Number of analyses	12				
<b>Spherulitic</b>						<b>Vermicular intergrowth (chlorite)</b>					
Mean value	1582	1356	20	0.07	0.06	Mean value	1580	1351	21	0.11	0.16
Std dev	0.9	3.2	1.5	0.07	0.09	Std dev	1.3	3.0	1.5	0.06	0.07
Number of analyses	15					Number of analyses	18				

G FWHM: Full width at half maximum of the G band

**Table 3** Results of the ion probe analysis (SIMS) of graphite morphologies. The  $\delta^{13}\text{C}$  values are relative to the PDB standard

<b>Vermicular intergrowths in chlorite</b>	$\delta^{13}\text{C}$ (‰)	<b>Cryptocrystalline</b>	$\delta^{13}\text{C}$ (‰)	<b>Flakes</b>	$\delta^{13}\text{C}$ (‰)
F2@1.asc	-34.87	P0@1.asc	-33.72	P0@17.asc	-29.26
F2@2.asc	-33.76	P0@2.asc	-32.56	P0@18.asc	-31.89
F2@3.asc	-33.99	P0@3.asc	-34.45	P0@19.asc	-28.97
F2@4.asc	-35.29	P0@5.asc	-34.09	P0@20.asc	-28.65
F2@5.asc	-34.20	P0@6.asc	-34.45	P0@21.asc	-29.72
F2@6.asc	-35.20	P0@7.asc	-33.87	P0@22.asc	-28.71
F2@7.asc	-35.15	P0@8.asc	-33.60		
F2@8.asc	-33.92	P0@9.asc	-31.60	G2C@1.asc	-30.85
F2@9.asc	-34.05	P0@10.asc	-32.10	G2C@2.asc	-31.31
		P0@11.asc	-34.29	G2C@3.asc	-30.56
<b>AVERAGE</b>	<b>-34.49</b>	P0@12.asc	-35.12	G2C@4.asc	-31.01
<b>Standard deviation</b>	<b>0.62</b>	P0@13.asc	-34.01	G2C@5.asc	-30.75
		P0@14.asc	-32.87	G2C@7.asc	-30.23
<b>Spherulites in chlorite</b>		P0@15.asc	-34.01	G2C@8.asc	-30.22
F2@11.asc	-29.87	P0@16.asc	-34.73	G2C@9.asc	-28.97
F2@12.asc	-30.02			G2C@10.asc	-31.55
F2@13.asc	-30.98	<b>AVERAGE</b>	<b>-33.70</b>	G2C@12.asc	-31.61
F2@14.asc	-29.76	<b>Standard deviation</b>	<b>1.00</b>		
F2@15.asc	-31.11			<b>AVERAGE</b>	<b>-30.26</b>
F2@16.asc	-29.18			<b>Standard deviation</b>	<b>1.10</b>
<b>AVERAGE</b>	<b>-30.15</b>				
<b>Standard deviation</b>	<b>0.75</b>				



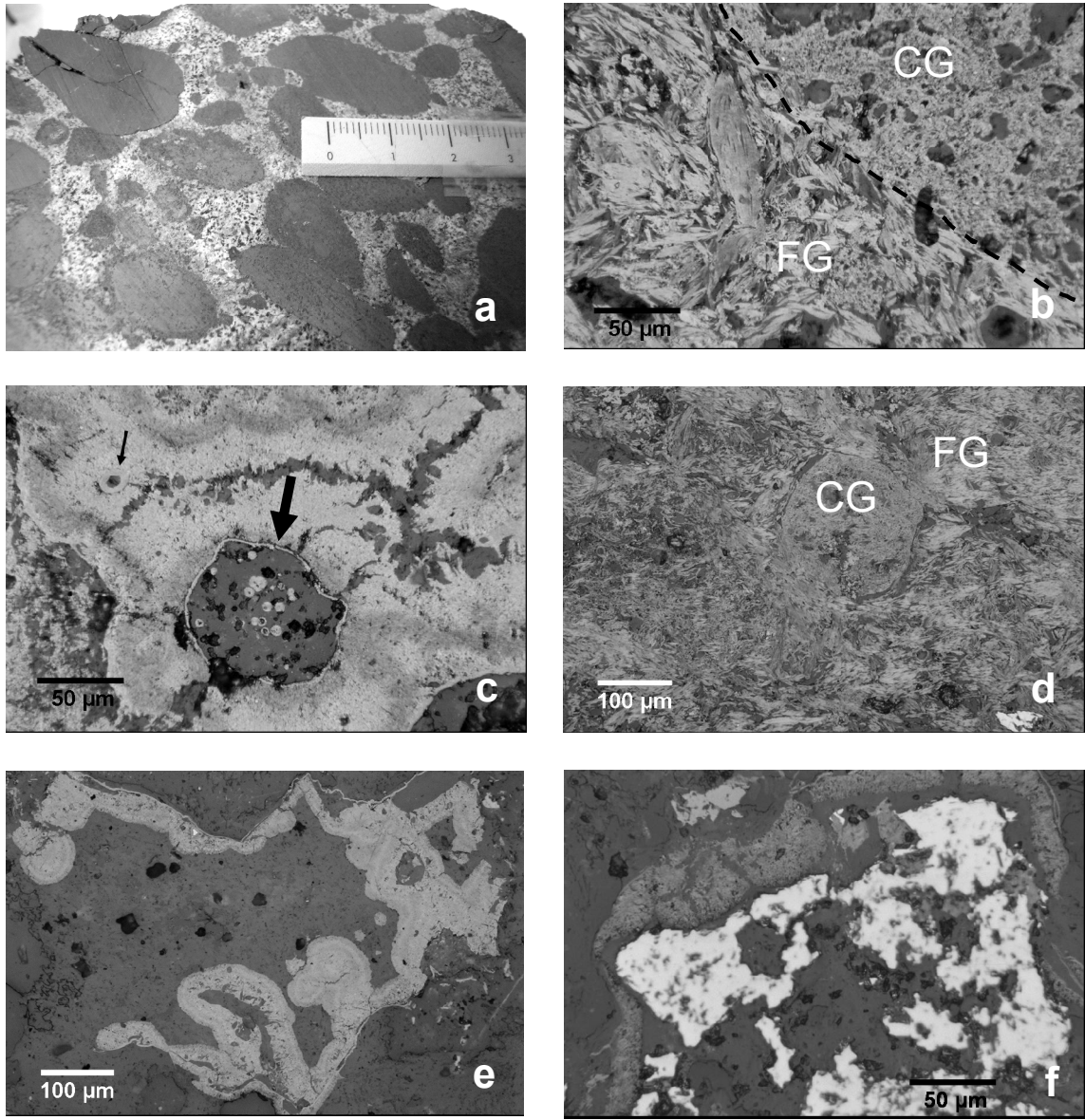


Fig.2

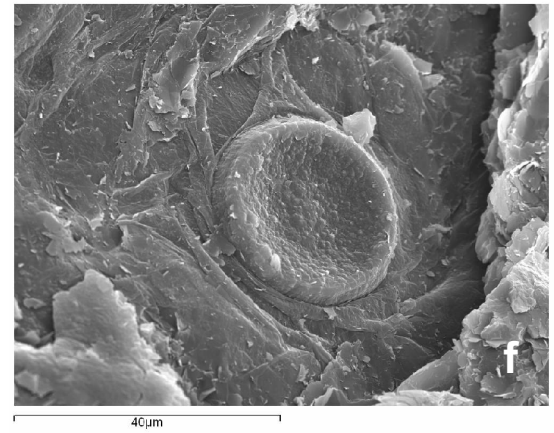
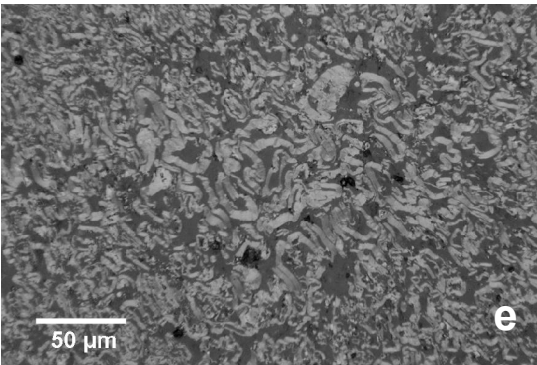
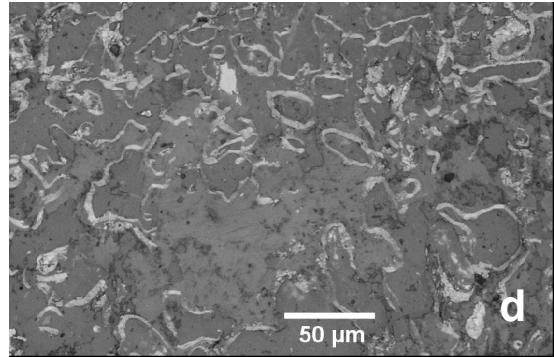
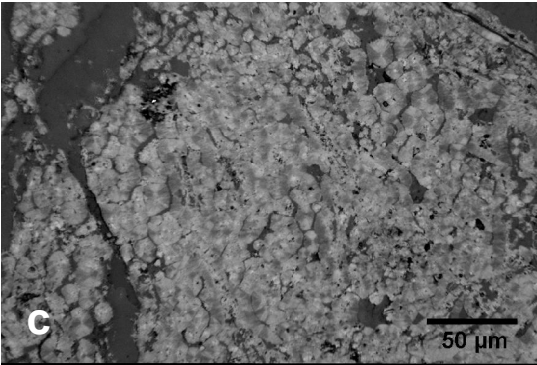
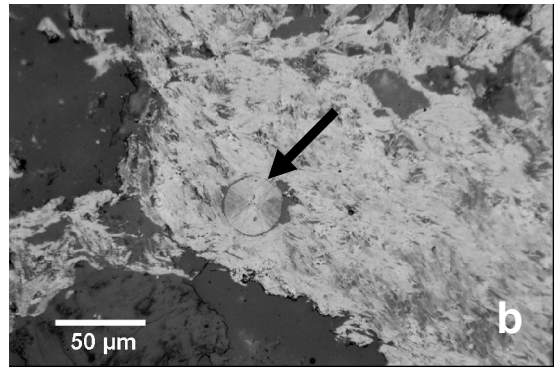
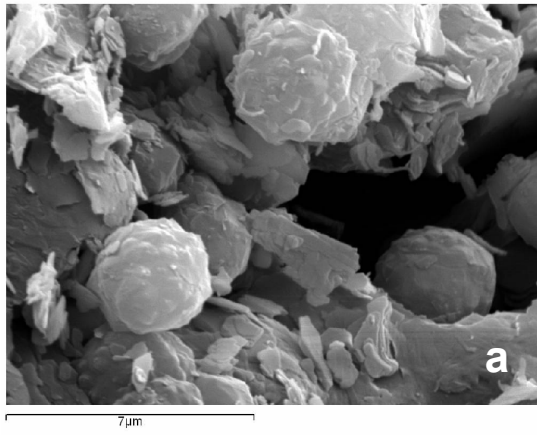


Fig.3

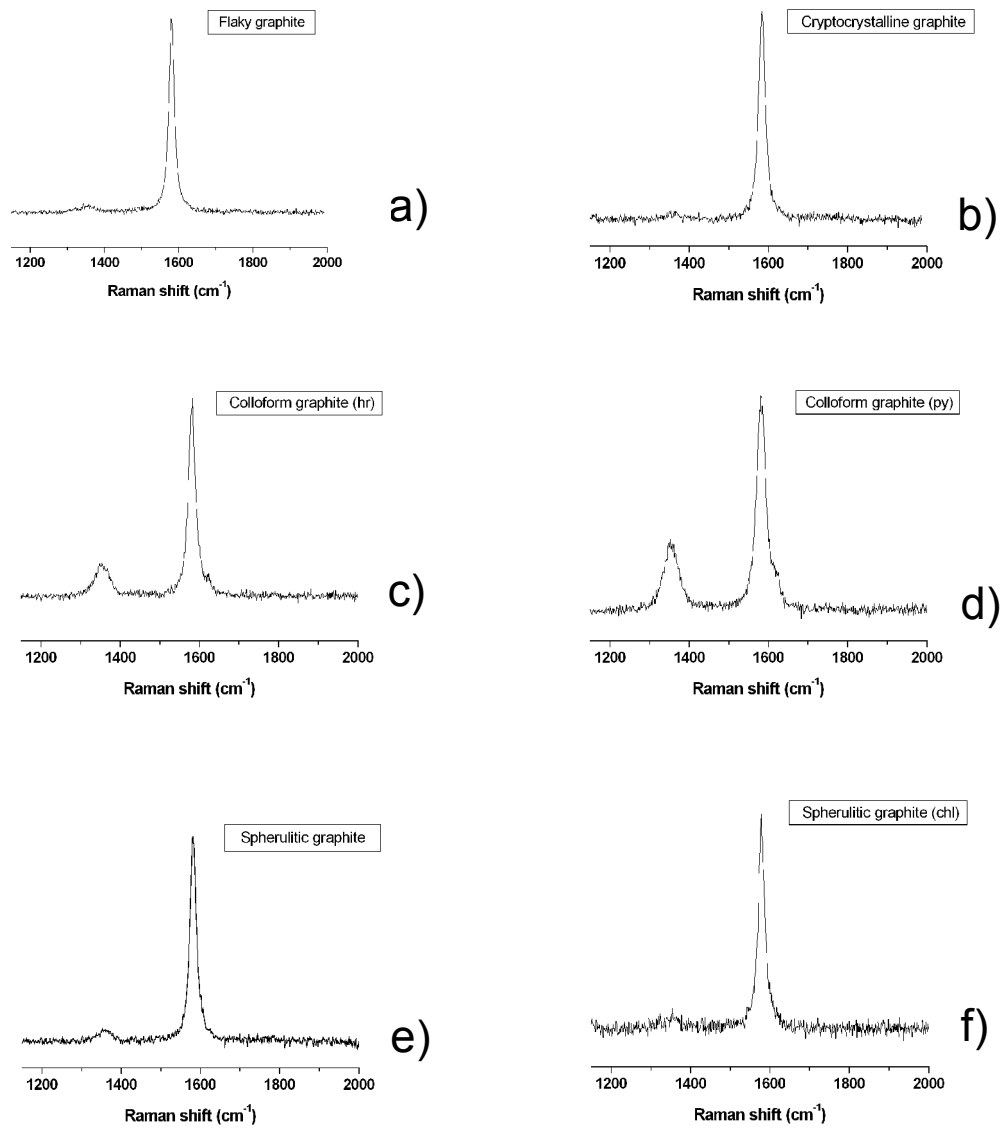


Fig. 4

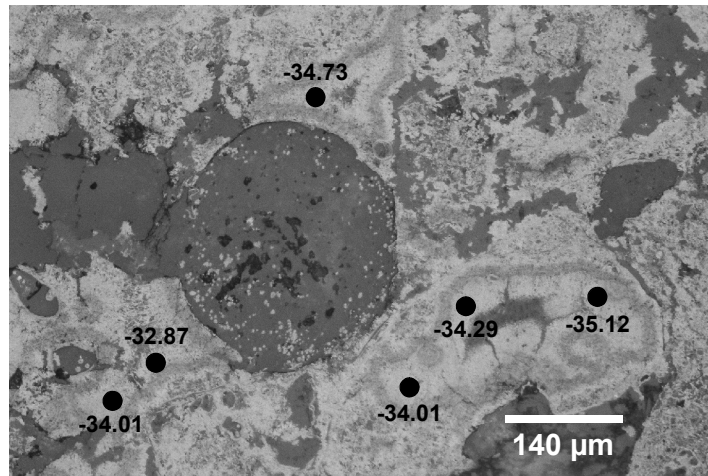


Fig. 5

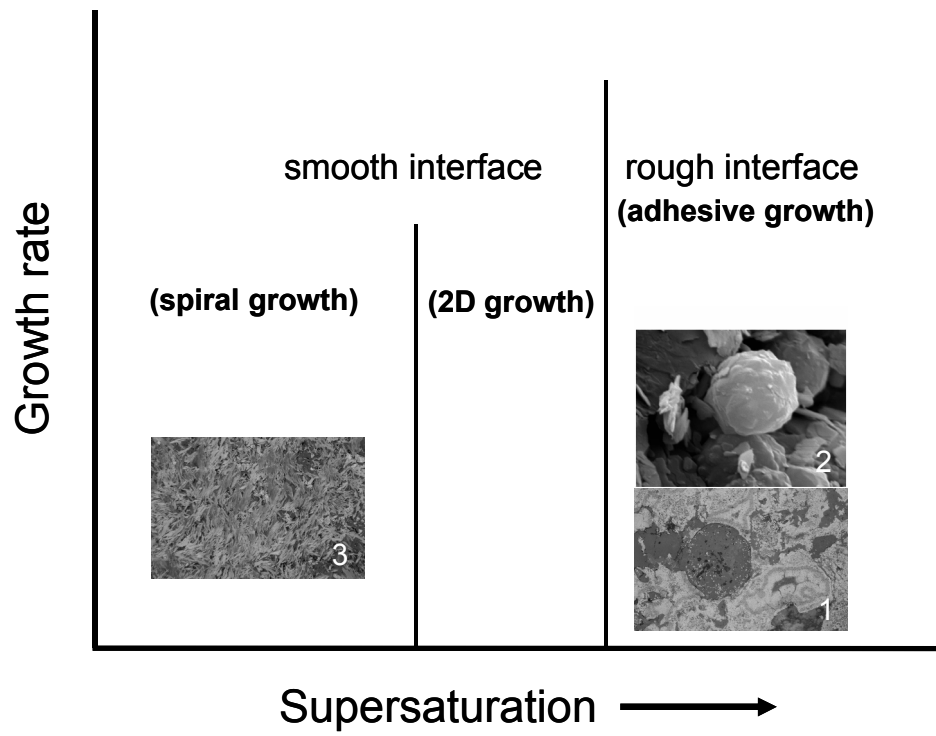


Fig. 6

